Int J Earth Sciences (Geol Rundsch) (2001) 90:412–425
DOI 10.1007/s005310000136

ORIGINAL PAPER

M. Schulz · D. Seidov · M. Sarnthein · K. Stattegger

Modeling ocean–atmosphere carbon budgets during the Last Glacial Maximum–Heinrich 1 meltwater event–Bølling transition

Received: 8 June 2000 / Accepted: 21 July 2000 / Published online: 22 November 2000

Abstract Benthic carbon isotope data indicate that the rate of North Atlantic Deep Water (NADW) formation and the mode of oceanic thermohaline circulation (THC) varied considerably across the transition from the Last Glacial Maximum (LGM) to the Heinrich 1 meltwater event (MWE) and, subsequently, to the Bølling warm period. We simulate changes in the Ocean–atmosphere carbon cycle induced by and linked to these oceanic fluctuations by means of a carbon cycle box model which resolves the major oceanic basins. The output from an ocean general circulation model (OGCM), which is forced by observed or reconstructed boundary conditions at its surface, serves to constrain the physical parameters of the carbon cycle model. The OGCM depicts three modes of Atlantic THC: an interglacial mode with vigorous NADW formation; a glacial mode with active, although weaker (–65%) NADW formation; and an MWE mode characterized by the complete lack of NADW formation. The carbon cycle model is forced from the LGM scenario into the MWE and finally into the Bølling interstadial. The glacial circulation mode accounts for approximately half (i.e., 37±3 µatm, depending on parameterization of biological productivity) of the observed glacial reduction in atmospheric CO_2 partial pressure (pCO_2). Approximately 70% of this pCO_2 decline is linked to changes in sea-surface temperature and salinity. The MWE circulation mode has only a small effect on atmospheric pCO_2 (±1 µatm) but goes along with a massive redistribution of carbon from the Indo-Pacific and Southern oceans to the Atlantic Ocean, which stores 85±8 Gt (gigatons) excess carbon during the MWE. The onset of NADW formation after a meltwater event, has the *potential* to release 81±6 Gt carbon from the model ocean to the atmosphere, corresponding to an atmospheric pCO_2 increase by 38±3 µatm, equivalent to approximately half of the modern, man-made pCO_2 load.

Keywords Last deglaciation · Carbon-cycle model · Ocean general circulation model · Oceanic carbon storage · Atmospheric carbon dioxide concentration · Paleoceanographic reconstruction

M. Schulz (✉) · M. Sarnthein · K. Stattegger
Institut für Geowissenschaften, Universität Kiel,
Olshausenstrasse 40, 24118 Kiel, Germany
E-mail: mschulz@email.uni-kiel.de
Phone: +49-431-8807324
Fax: +49-431-8801569

D. Seidov
Earth System Science Center, Pennsylvania State University,
248 Deike Bldg., University Park, PA 16802–2711, USA

Introduction

Based on high-resolution benthic $\delta^{13}C$ and Cd/Ca data obtained from deep-sea sediment cores, it has been postulated that the large-scale oceanic thermohaline circulation patterns varied considerably during the transition from the last glacial maximum (LGM) to the Holocene (Boyle and Keigwin 1987; Duplessy et al. 1988; Keigwin et al. 1991; Boyle 1992; Charles and Fairbanks 1992; Sarnthein et al. 1994). In particular, these paleoceanographic data imply that different modes of Atlantic thermohaline circulation (THC) were realized in the past. Presently, the formation of deep water in the North Atlantic leads to a vigorous THC in the Atlantic and to an export of ~14 sverdrups (Sv; 1 Sv=10^6 m^3 s^{-1}) of North Atlantic Deep Water (NADW) to the Southern Ocean (Schmitz 1995). For the LGM paleoceanographic proxy data indicate that the THC in the Atlantic was approximately 30% weaker (Sarnthein et al. 1994) or even as strong as at present (Yu et al. 1996). A contrasting picture emerges from proxy data for the early stage of the last deglaciation between ~17 and 14.7 cal. ky B.P.

(10^3 calendar years before present). During this time interval the initial disintegration of the Barents Sea ice sheet and the massive release of icebergs from the Laurentide ice sheet during Heinrich event 1 delivered large amounts of meltwater to the North Atlantic (Jones and Keigwin 1988; Lehman et al. 1991; Bond et al. 1992; Sarnthein et al. 1992, 1995, in press). The Heinrich 1 meltwater event resulted from an overlap of at least two separate major surges, an early surge from Labrador and a later surge from the Barents shelf, in addition to initial surging from East Greenland. Based on spatial $\delta^{18}O$ anomalies in surface water, the most pronounced meltwater injection is registered in the northeastern Norwegian Sea (Sarnthein et al., in press). The resulting meltwater lid had a profound effect on the THC in the Atlantic, since it inhibited the formation of NADW (Sarnthein et al. 1994; Seidov et al. 1996; Seidov and Haupt 1997, 1999). According to these authors, the Heinrich 1 meltwater event (MWE) was characterized by a weak reversed THC in the Atlantic, largely driven by deep-water formation in the Southern Ocean.

Sarnthein et al. (1994) estimated the amount of carbon stored in the eastern Atlantic during the last 33 cal. ky from benthic $\delta^{13}C$ data. They concluded that, relative to the modern situation, ~40 Gt (gigatons) and ~70 Gt excess carbon were stored in this basin during the LGM and MWE. The additional carbon storage during the LGM comprises ~25% of the difference in atmospheric carbon content between the LGM and pre-industrial time (Barnola et al. 1987; Neftel et al. 1988). These observations raise the question as to whether the extent to which variations in atmospheric CO_2 partial pressure (pCO_2) that occurred during the transition from the LGM to pre-industrial times were caused by variations in carbon storage in the Atlantic and in other ocean basins, all triggered by different intensities of the Atlantic THC.

Based on a four-box model, Siegenthaler and Wenk (1984) suggested that abrupt changes in ocean circulation strength can induce significant variations in atmospheric pCO_2 on a centennial time scale. According to this study a reduction in vertical oceanic mixing at high latitudes by 50% causes a pCO_2 drop of ~50 µatm; however, since the model does not distinguish deep-water formation in the North Atlantic from that in the Southern Ocean, the relevance of the modeled pCO_2 variations for the last deglaciation is unclear. Subsequent modeling studies (Keir 1988; Michel 1991; Heinze and Hasselmann 1993; Heinze 1994; Paillard et al. 1993) showed that at steady state atmospheric pCO_2 decreases by ~10–30 µatm upon halving the NADW formation rate or appeared to be insensitive to glacial-to-interglacial circulation changes (Winguth et al. 1999). This view was challenged by Marchal et al. (1998) who simulated a net pCO_2 increase during the transient collapse of the present-day NADW formation.

In this study we investigate the effect of THC changes on atmospheric pCO_2 during the early part of the last deglaciation by a biogeochemical box model which is forced by the output from a global ocean general circulation model (OGCM). Our experiments are not intended to simulate the full glacial-to-interglacial change in atmospheric pCO_2, but to assess potential effects of deglacial changes in NADW formation rate on the carbon distribution in the ocean–atmosphere system. After a description of the model setup and a brief overview of the OGCM results, various carbon cycle scenarios are explored.

Model setup

We use the Modular Ocean Model (Bryan 1969; Cox 1984; Pacanowski et al. 1993) in a global configuration with a horizontal resolution of 6×4 (longitude×latitude) and 12 layers in the vertical. The model is forced by restoring boundary conditions for sea-surface temperature (SST) and salinity (Table 1). Details of the model setup are given by Seidov et al. (1996) and Seidov and Haupt (1999).

The carbon-cycle model is realized as box model. The oceanic part comprises five box stacks, each consisting of a surface box and 11 subsurface boxes with interface depths identical to the OGCM layers. Zonal boundaries of the box stacks are selected on the basis

Table 1 Ocean general circulation model (OGCM) boundary conditions. Whenever available, the mean of summer and winter data is used. *SST* sea-surface temperature; *SSS* sea surface salinity

Modern; MOD	SST	Levitus and Boyer (1994), as in Seidov and Haupt (1999)
	SSS	Levitus et al. (1994), as in Seidov and Haupt (1999)
	Wind	Lorenz et al. (1996), as in Seidov and Haupt (1999)
Last Glacial Maximum (17.1–21 cal. ky B.P.); LGM	SST	As in Seidov and Haupt (1999), modified according to new Kiel data
	SSS	Seidov and Haupt [1999; modified to enhance intermediate water formation in the North Pacific (Duplessy et al. 1988)]; supplemented by data from Duplessy (1982) and Duplessy et al. (1996)
	Wind	Lorenz et al. (1996), reduced by 25% south of 40°S (sea-ice screening)
Heinrich 1 meltwater event (14.7–17.1 cal. ky B.P.); MWE	SST	North Atlantic: as in Seidov et al. (1996); elsewhere: as for LGM
	SSS	North Atlantic: as in Seidov et al. (1996); elsewhere: as for LGM
	Wind	As for LGM

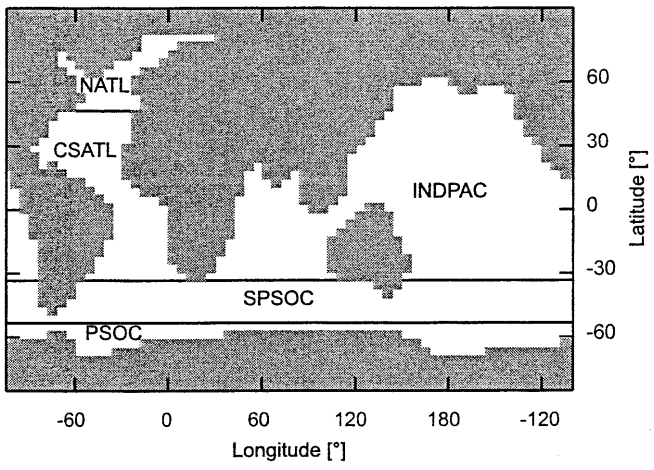

Fig. 1 Land–sea distribution in the OGCM and boundaries of box stacks in the carbon cycle box model (*solid lines*). *NATL* North Atlantic; *CSATL* Central/South Atlantic; *SPSOC* subpolar Southern Ocean; *PSOC* polar Southern Ocean; *INDPAC* Indo-Pacific

of the modeled meridional overturning of the OGCM (Fig. 1). To resolve the formation of NADW, we separate the North Atlantic (NATL) box stack from the Central/South Atlantic (CSATL). Similarly, the Southern Ocean is separated into a subpolar (SPSOC) and a polar (PSOC) domain, to resolve deep-water formation in the latter. Because of their common overturning pattern (with respect to the SPSOC) we combine the Indian and Pacific oceans into a single box stack (INDPAC).

Following basic box-modeling concepts (e.g. Keeling and Bolin 1967; Bolin 1981), the model predicts the concentrations of the following tracers in the ocean: total dissolved inorganic carbon (DIC); stable ($DI^{13}C$) and radioactive ($DI^{14}C$) carbon isotopes; total alkalinity (ALK); and phosphate (PO_4). Tracer concentrations are normalized to mean ocean salinity, thus avoiding an explicit consideration of surface freshwater fluxes. Isotope ratios in delta notation are diagnosed from concentrations of total carbon and the respective isotope.

Net water transports between the boxes are obtained by integration of OGCM velocities across the box boundaries. Oceanic mixing processes are explicitly included in the box model: Vertical mixing due to standing eddies is derived from the lateral variability of the OGCM transport around the net transport for each depth-interface of the box model, whereas vertical tracer transport by transient eddies is parameterized as diffusive process (diffusivity=0.4 $cm^2 s^{-1}$). Convection at high latitudes is parameterized as continuous mixing process between adjacent boxes with a mixing time scale of 1 year. Box stacks, where convection takes place and the depths to which convection penetrates from the surface are prescribed, based on the spatial and temporal distribution of convective adjustment events in the OGCM. Basin scale horizontal mixing is represented by depth-dependent horizontal diffusion (after Stocker et al. 1994).

In the atmospheric box partial pressures of total CO_2 (pCO_2) and carbon isotopes ($p^{13}CO_2$ and $p^{14}CO_2$) are predicted. The exchange of carbon across the ocean–atmosphere boundary is parameterized as linear gradient flux, taking into account variable isotopic fractionation during gas exchange (Zhang et al. 1995). Aqueous pCO_2 in the surface layer is determined from DIC and ALK (Peng et al. 1987) after de-normalizing salinity-normalized concentrations. Temperatures and salinities of the topmost OGCM layer are used to calculate temperature- and salinity-dependent parameters in the box model.

Biological export production in the surface layers (Q_{bio}) occurs at a constant "Redfield ratio" (Anderson and Sarmiento 1994) and is limited by the availability of PO_4. For the modern control experiment, export production in each surface layer is diagnosed by restoring PO_4 concentrations ($[PO_4]$) to observed values ($[PO_4]_{obs}$); cf. Najjar et al. 1992):

$$Q_{bio} = \frac{r_{C:P}}{\tau}\left([PO_4] - [PO_4]_{obs}\right)V, \quad (1)$$

where $r_{C:P}$=117 is the molar Redfield ratio between carbon and phosphate, τ=0.1 year is a restoring time scale, and V denotes the volume of the surface layer. In contrast, export production in paleoclimate experiments depend on PO_4 concentration according to Michaelis-Menten kinetics (Dugdale 1967):

$$Q_{bio} = r_{C:P}\frac{\omega[PO_4]}{k_m + [PO_4]}, \quad (2)$$

with phosphate uptake rate ω and k_m=2.5·10^{-4} mol m^{-3} (Lalli and Parsons 1993). Using the export production after Eq. (1) for the modern control run, ω can be derived from Eq. (2). The production ratio between calcareous shells and organic matter varies with temperature (after Heinze 1990) and the isotopic composition of organic matter depends on CO_2 concentration (Jasper et al. 1994). Since the model contains no sediment reservoir, all particles leaving the surface layer are remineralized at depth, using different depth scales for remineralization of organic matter and calcareous shells.

Initial oceanic conditions are based on GEOSECS data (Bainbridge 1981, 1982a, 1982b) and atmospheric initial values are taken from ice-core data (Barnola et al. 1987). Overall the model reproduces observed vertical and horizontal oceanic tracer gradients fairly well (Schulz 1998). Production of organic matter amounts to 9.9 Gt C year^{-1} and ~1.2 Gt C year^{-1} leave the surface ocean in biogenic carbonate shells.

Throughout the text we use the term modern (MOD) as a synonym for preindustrial with respect to the carbon cycle and for present-day with respect to the ocean circulation.

OGCM results

Modern meridional overturning (Fig. 2a) is in good agreement with the deduced large-scale circulation pattern of the modern oceans. The Atlantic Ocean is dominated by the formation of North Atlantic Deep Water (NADW) with an associated maximum volume transport of 21.5 Sv; 9.5 Sv NADW are exported to the Southern Ocean. Whereas the maximum overturning corresponds with oceanographic estimates, the NADW outflow from the Atlantic Ocean is underestimated (Schmitz 1995; Macdonald and Wunsch 1996) and occurs ~500 m too shallow (Reid 1996). The model forms 8 Sv Antarctic Bottom Water (AABW) that flows into the Atlantic Ocean. This modeled AABW flux agrees with the upper bound of oceanographic estimates (Macdonald 1993; Schmitz 1995). Meridional overturning in the combined Indian and Pacific oceans is characterized by a single cell with 35-Sv inflow at depth and corresponding near-surface outflow.

The glacial meridional overturning pattern in the Atlantic Ocean (Fig. 2b) shows the same basic structure as in the control experiment (Fig. 2a), including

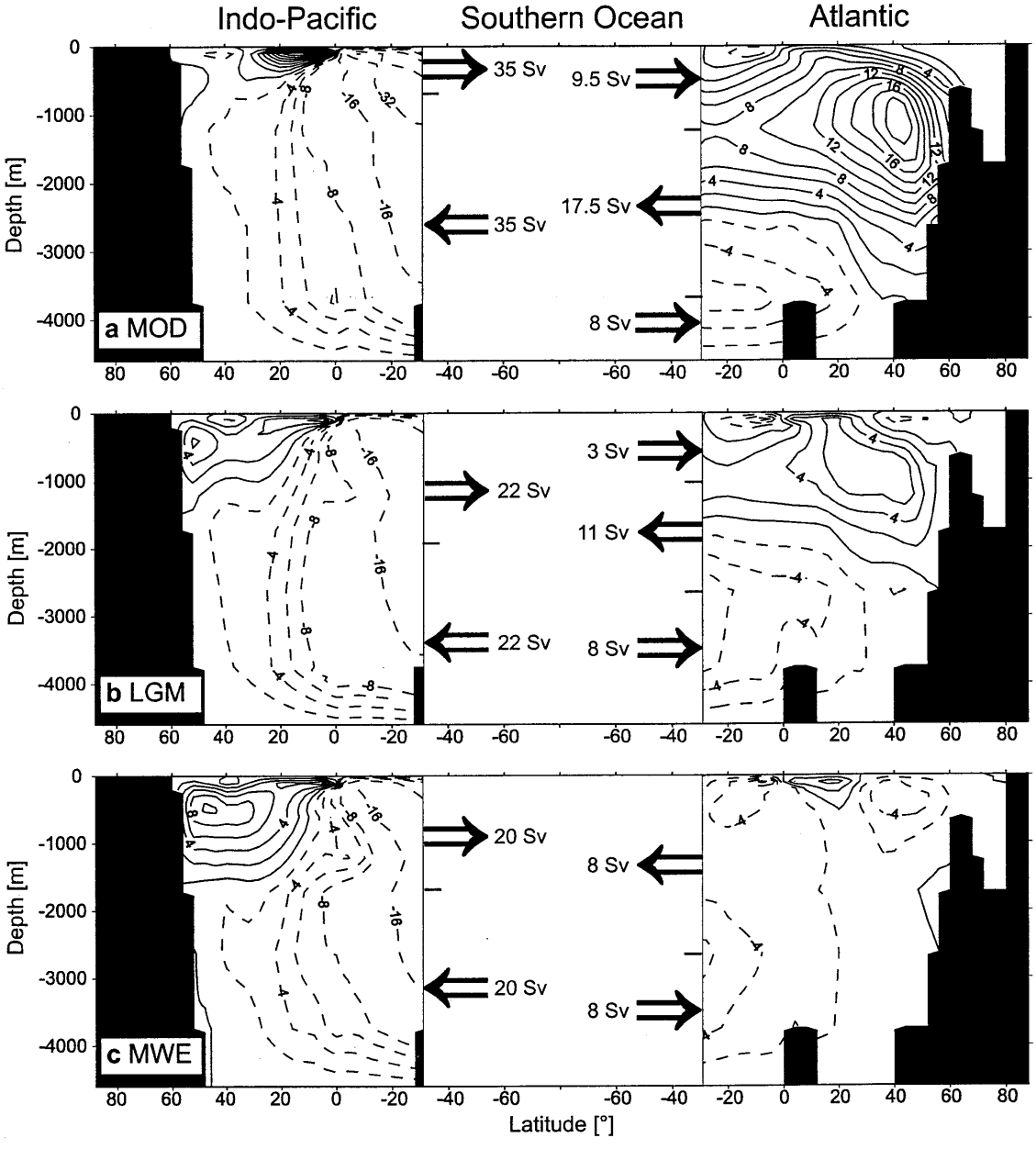

Fig. 2 Zonally integrated meridional mass transport stream function in the Atlantic and the combined Indian and Pacific oceans for **a** modern situation (*MOD*), **b** Last Glacial Maximum (*LGM*) and **c** Heinrich 1 meltwater event (*MWE*). Contours in Sv (1 Sv=10^6 m^3 s^{-1}); positive values denote clockwise rotation in the Atlantic and counter-clockwise rotation in the Indo-Pacific oceans. *Arrows* at 32°S indicate net transports into and out of the Southern Ocean

NADW formation and bottom-water inflow from the Southern Ocean. The major differences between the two experiments for the Atlantic Ocean comprise the following:

1. A reduced rate of NADW formation. The associated maximum volume transport in the North Atlantic amounts to 7.5 Sv and is, thus, much weaker than in the control experiment (21.5 Sv).
2. The export of NADW to the Southern Ocean decreases from 9.5 Sv in the control run to 3 Sv in the LGM experiment.
3. The interface between NADW and AABW moves upward by ~800 m.

Compared with experiments conducted by Seidov et al. (1996), the additional consideration of a negative sea-surface salinity anomaly in the Southern Ocean (Table 1; Duplessy et al. 1996) leads to more pronounced weakening of glacial NADW formation. Total transport between the Southern Ocean and the combined Indo-Pacific Ocean falls from 35 Sv in the control experiment to 22 Sv in the LGM run (Fig. 2a,b).

The modeled LGM circulation pattern is consistent with paleoceanographic data which indicate a shallowing of the NADW layer and a more northerly penetration of AABW as compared with the present (Boyle and Keigwin 1987; Oppo and Fairbanks 1987; Duplessy et al. 1988; Sarnthein et al. 1994); however, the core of modeled NADW appears ~800 m shallower than in the LGM reconstructions by Sarnthein et al. (1994). As for the control experiment, we attribute this discrepancy to the low vertical resolution of the OGCM. Yu et al. (1996) postulated that NADW export to the Southern Ocean remained at its Holocene rate during the LGM. This contrasts with our model results, which indicate a weakening in glacial NADW export by –68%. This modeled reduction matches similar figures obtained in other modeling studies [Duplessey et al. 1996 (–75%); Ganopolski et al. 1998 (–66%); Weaver et al. 1998 (–63%); estimated from the published zonally integrated meridional mass transport stream functions]. The simulation of Campin et al. (1999) suggests a somewhat smaller reduction by 53%, whereas Winguth et al. (1999) obtain an even stronger decrease by 83%. Furthermore, an experiment with a coupled atmosphere-ocean-model indicates a strengthening of glacial AABW inflow into the Atlantic by 1.5 Sv (Ganopolski et al. 1998), whereas our results with an ocean only model do not indicate this trend. A likely explanation is that in our model the density increase, linked to glacial cooling of the Southern Ocean surface water, is counterbalanced by the negative salinity anomaly.

In the MWE experiment, the large negative sea-surface salinity anomaly in the North Atlantic inhibits deep convection in this area and leads to a complete cessation of NADW formation (Fig. 2c). Hence, the modeled MWE circulation pattern in the Atlantic differs fundamentally from the LGM and modern mode (Sarnthein et al. 1994; Seidov et al. 1996; Seidov and Haupt 1997, 1999). Below ~500 m depth the entire Atlantic is dominated by water masses, which originate in the Southern Ocean. These model results are consistent with inferences drawn from paleoceanographic proxy data (Keigwin et al. 1991; Sarnthein et al. 1994).

The MWE circulation pattern for the Indo-Pacific is almost identical to the glacial pattern, since OGCM boundary conditions remain unchanged in these oceans. However, compared with the LGM run, the increase of sea-surface salinity in the Northwest Pacific leads to a further intensification of intermediate-water formation and is consistent with enhanced intermediate-water ventilation during Heinrich Events in the North Pacific (Berger 1977; Duplessy et al. 1989; Kennett and Ingram 1995).

Carbon cycle scenarios

Experimental strategy

Since reconstructed boundary conditions for the OGCM are available only for selected time intervals, we must make use of additional paleoceanographic information to obtain a forcing set for the carbon cycle model which is continuous in time over the time span of early deglaciation. For this purpose we treat the results of the three OGCM experiments as basic modes of operation (strong, weak, and no NADW formation) of the thermohaline circulation. On the other hand, various benthic $\delta^{13}C$ and Cd/Ca time series provide a continuous proxy record of NADW history over the last deglaciation (Boyle and Keigwin 1987; Jansen and Veum 1990; Charles and Fairbanks 1992; Sarnthein et al. 1994; Marchitto et al. 1998). Per analogy, we proceed by describing a (time-dependent) continuous NADW history by linear interpolation between the OGCM results for the three circulation modes. Accordingly, our model setup cannot capture the transient response of the ocean–atmosphere carbon cycle during the Heinrich event 1 meltwater perturbation.

Starting from the LGM steady state, we switch to MWE boundary conditions at 17.1 cal. ky B.P. using a transition time of 10 years. The abruptness of this transition reflects OGCM results, according to which the actual shutdown of NADW formation upon freshwater input at high latitudes occurs on a decadal time scale ("convective instability"; Bryan 1986; Rahmstorf et al. 1996). In harmony with deep-sea records (Sarnthein et al. 1994) the model is forced with MWE boundary conditions from 17.1 to 14.7 cal. ky B.P.

The lack of a particular OGCM experiment for the Bølling makes it necessary to employ the modern control run as surrogate for this climatic warm period. The rationale behind this step is based on the observation that proxy data from the North Atlantic realm

indicate that the Bølling period was only slightly colder than the present temperature (SST: Duplessy et al. 1992; Lehman and Keigwin 1992; Koç Karpuz and Jansen 1992; Schulz 1995; Veum et al. 1992; air temperature: Atkinson et al. 1987; Dansgaard et al. 1993; Guiot et al. 1993). The associated northward heat transport was probably linked to NADW formation on an interglacial level (Sarnthein et al. 1994). The selection of the transition time from the MWE to the Bølling (=MOD) state is somewhat arbitrary. Experiments with a coupled ocean–atmosphere model (Manabe and Stouffer 1995) suggest that the reinitiation of NADW formation after a massive freshwater input into the North Atlantic occurs within a few centuries; therefore, we assume a transition time of 150 years and keep the carbon cycle model in the Bølling state until 13.0 cal. ky B.P. In the real world, however, the switch may have occurred on a decadal time scale (=time span of snow-accumulation change on Greenland; Alley et al. 1993).

Evolution of export production and atmospheric pCO_2

In an initial experiment A (Table 2), we used the diagnostic modern PO_4 uptake rates (ω in Eq. 2) to predict export production during the LGM and MWE. This implies that marine ecosystem dynamics, which are parameterized by the PO_4 uptake rates, do not vary on glacial-to-interglacial time scales, in contrast to paleoceanographic reconstructions (Sarnthein et al. 1988). Compared with the modern pCO_2 level of 280 µatm, glacial pCO_2 is reduced by 36 µatm (Fig. 3a). Approximately 29 µatm of this reduction is caused by changes in SST and salinity, which enhance the CO_2-solubility pump. The glacial circulation pattern alone lowers pCO_2 by another ~24 µatm; however, this pCO_2 decrease is largely compensated by a concomitant drop in export production (discussed below), which raises pCO_2 by 17 µatm.

After the transition to MWE boundary conditions, atmospheric pCO_2 increases, reaching a value of ~1 µatm above the glacial level at 14.7 cal. ky B.P. During the subsequent transition to the Bølling, pCO_2

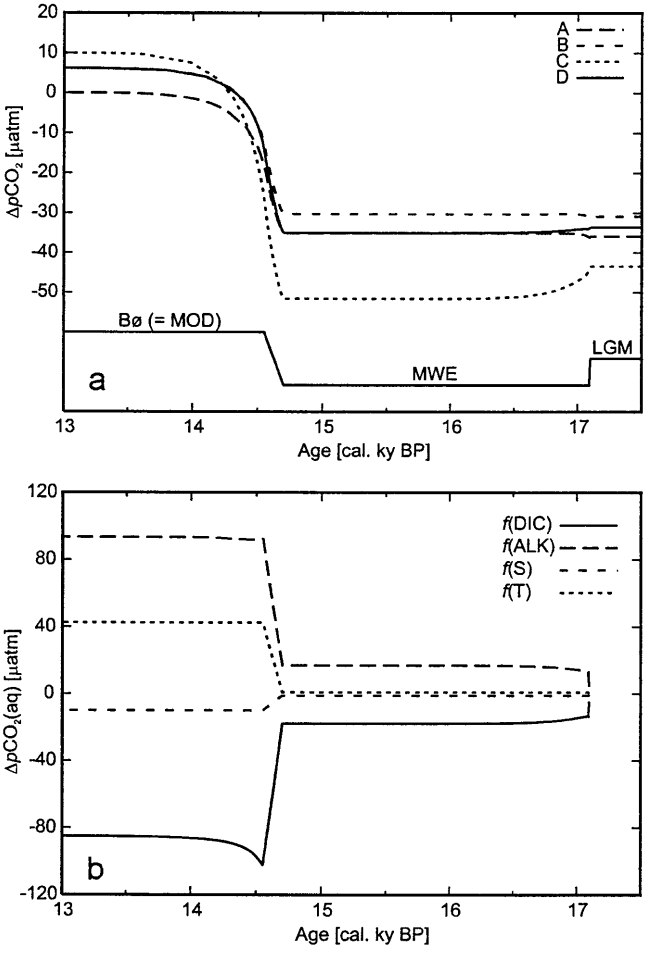

Fig. 3a,b Changes in CO_2 partial pressure. **a** Deviation of atmospheric pCO_2 from pre-industrial value of 280 µatm in experiments A–D (*A* modern PO_4 uptake rates; *B* increased mean tracer concentrations; *C* modern productivity; *D* reconstructed glacial productivity; cf. Table 2). *Bottom curve* schematically shows the forcing of the carbon-cycle model using three basic modes of thermohaline circulation (*Bø* Bølling). **b** Deviation of globally integrated aqueous pCO_2 from LGM value as function of changes surface-water *DIC*, *ALK*, temperature (*T*) and salinity (*S*). Dependence of $pCO_2(aq)$ on PO_4 is always <0.4 µatm and therefore not shown. See text for further details

Table 2 Summary of carbon cycle model experiments. *MOD* modern; *LGM* Last Glacial Maximum; *MWE* Heinrich 1 meltwater event

Experiment	Setting
A	MOD: productivity from diagnosed PO_4 uptake rates LGM/MWE: productivity prognosticated (modern PO_4 uptake rates)
B	As in A, but all mean tracer concentrations increased by 3%
Mean tracer concentrations increased by 3% in experiments C–F	
C	Prescribed modern productivity (from A)
D	LGM: prescribed productivity MWE: productivity prognosticated (glacial PO_4 uptake rates from D) MOD: productivity prognosticated (modern PO_4 uptake rates from A)
E	As in D; in addition, "warm" Southern Ocean during MWE and "cold/salty" Bølling
F1,2,3	As in E; in addition, terrestrial carbon uptake (0.1, 0.2 and 0.3 Gt C $year^{-1}$) during Bølling

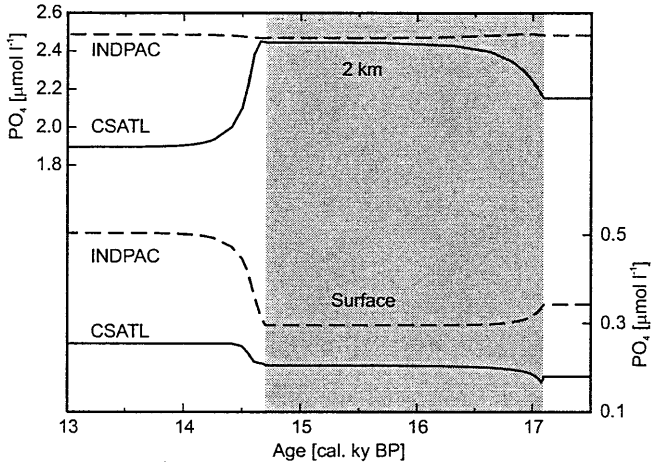

Fig. 4 Modeled variation in PO_4 concentration in the CSATL (*solid lines*) and INDPAC (*dashed lines*) in 2 km depth (*top*) and surface layer (*bottom*). *Shading* shows duration of MWE

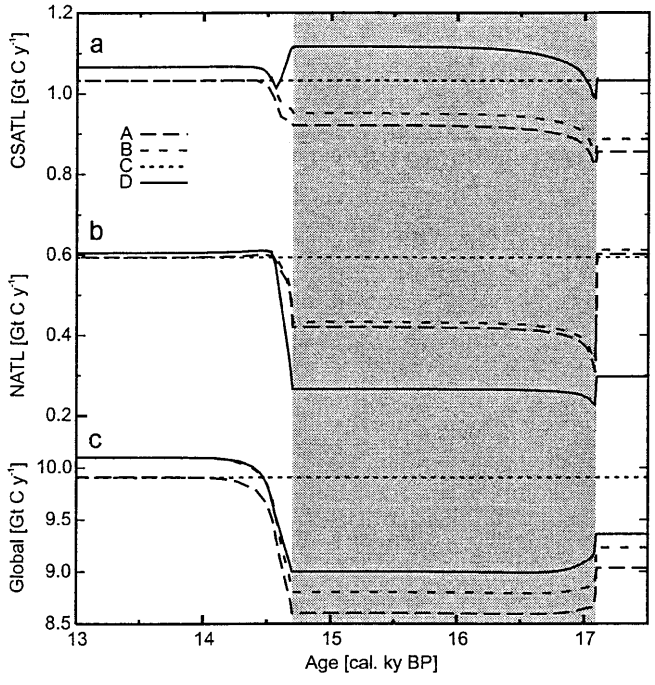

Fig. 5 Biological export production in experiments A–C in **a** CSATL, **b** NATL and **c** globally integrated. *Shading* shows duration of MWE

rises to the modern value on a centennial time scale. Thus, despite the fundamental change in the rate of NADW formation, the model predicts only a marginal effect of the Heinrich 1 meltwater event on atmospheric pCO_2. This model behavior largely results from changes in the sites and modes of biological carbon fixation, caused by a net transfer of PO_4 from the Indo-Pacific and Southern Ocean to the Atlantic Ocean during the LGM-to-MWE transition. Accordingly, PO_4 concentrations increase considerably in the deep CSATL (14%) and decrease slightly in the deep INDPAC (1%; Fig. 4). Contemporaneously, PO_4 concentrations in the surface water drop everywhere but in the CSATL (Fig. 4), causing a decrease in global export production by 1.3 Gt C $year^{-1}$ (–13%; Fig. 5c) compared with the modern value. Sediment records indeed depict a general early decrease in paleoproductivity right at the end of the LGM or slightly earlier (Sarnthein et al. 1988). Reduced biological carbon fixation provides a negative feedback on atmospheric pCO_2 and largely counterbalances the enhanced carbon storage in the deep Atlantic Ocean which parallels the increase in PO_4 storage (Fig. 4; cf. Ocean atmosphere carbon budgets).

In experiment A the model predicts a glacial reduction in productivity by 9% globally and by 10% in the combined NATL and CSATL (Fig. 5, exp. A). This result is at odds with paleoceanographic data, which suggest an increase in glacial productivity at least in the Atlantic Ocean and possibly on a global scale (Sarnthein et al. 1988; Mix 1989). Since productivity in the model is limited by the availability of PO_4, it follows that the amount of PO_4 transported into the surface layers is not sufficient to increase glacial productivity above the modern level. Possible reasons for this shortcoming are:

1. A change in mean PO_4 concentration, linked to the late-glacial reduction in ocean volume (Fairbanks et al. 1992) is neglected.
2. Possible variations in glacial ecosystem dynamics, which might alter the PO_4 uptake rates, are ignored.
3. The glacial circulation pattern is insufficient to transport the required amount of PO_4 into the surface layers (e.g. seasonal effects are not resolved).
4. Both the southern and northern low-latitude upwelling zones along the Atlantic and Indo-Pacific eastern continental margins are all fed by water upwelled from the upper intermediate level (at ca. 400–700 m depth) from the Southern Ocean, a special advection track poorly resolved in coarse-resolution OGCMs.

To assess the effect of sea-level induced variations of mean tracer concentrations, we increased the amount of all tracers in the model by 3% during the entire LGM-to-Bølling transition (exp. B). Despite this modification, the model still predicts a decrease in global productivity by 7% for the LGM (Fig. 5c). Hence, variations of mean tracer concentrations alone cannot compensate for the reduction in glacial productivity caused by lowered PO_4 concentrations in the surface ocean. The resulting pCO_2 evolution parallels that of experiment A (Fig. 3a) but is offset by ~5 µatm. The offset varies slightly in time due to the nonlinear dependency of aqueous pCO_2 on ALK and DIC concentrations. In the following experiments, we fixed the mean concentrations at the elevated level of experiment B, since this may constitute a good approximation to the early deglacial regime.

To estimate the pure effect of changes in ocean circulation on atmospheric pCO_2 in the absence of the negative feedback provided by the concomitant reduction in productivity, we conducted experiment C with prescribed modern export productivities. Although this experiment yields negative PO_4 concentrations in some surface boxes, it is nevertheless instructive because it allows us to assess the strength of the "productivity feedback". Compared with experiment B, elevated productivity during the LGM reduces atmospheric pCO_2 by an additional 13 μatm (Fig. 3a). However, the most important difference occurs during the MWE, where a decrease by up to 8 μatm relative to the glacial level replaces the slight increase in pCO_2, observed in experiments A and B. During the Bølling atmospheric pCO_2 exceeds the level of experiment A, because the elevated DIC and ALK concentrations raise the mean aqueous pCO_2 in the surface ocean. For comparison, in experiment B higher global productivity during the Bølling (Fig. 5c), which is linked to elevated mean PO_4 concentration, leads to a smaller atmospheric pCO_2 level than in experiment C.

To exploit the most realistic changes in productivity during the LGM-to-Bølling transition, we prescribed glacial export productivities based on paleoceanographic reconstructions and use the resulting glacial PO_4 uptake rates to predict productivity during the MWE (exp. D): For the LGM we assume a reduction in productivity relative to experiment A by 50% in polar regions (NATL and PSOC; Sarnthein et al. 1988; Manighetti and McCave 1995; Nürnberg et al. 1997) and modern productivity (from exp. A) elsewhere. The latter setting contrasts paleoceanographic data, which indicate an increase in glacial productivity in the CSTAL by at least 20% (Sarnthein et al. 1988; Mix 1989). However, the amount of PO_4 transported into the surface layer of the CSATL by the glacial circulation is insufficient to allow for a productivity increase above the modern level. Although glacial productivity in some regions of the Indo-Pacific Ocean (INDPAC) was presumably higher than at present (Lyle 1988; Sarnthein et al. 1988; Pedersen et al. 1991; Sancetta 1992; Murray et al. 1993; Herguera and Berger 1994), it is not yet apparent whether this is also true for overall productivity in these oceans; therefore, we made the conservative assumption that glacial productivity in the INDPAC remains at its modern level. For the SPSOC recent paleoceanographic data are contradictory, indicating either an extreme increase in productivity (Kumar et al. 1995) or overall constant productivity associated with a northward shift of the high productivity belt because of the migration of the polar front (Francois et al. 1997; Nürnberg et al. 1997). Accordingly, we made a conservative choice as for the INDPAC and prescribed productivity at a modern level for the glacial SPSOC. Finally, export production during the Bølling is prognosticated using modern PO_4 uptake rates from experiment A.

Compared with experiment B, the modification of biological carbon fixation in experiment D results in a drop of glacial atmospheric pCO_2 by ~3 μatm (Fig. 3a) which is caused by the increase in global export production by ~0.1 Gt C years^{-1} (Fig. 5c). During the transition to the MWE, global productivity drops less pronounced than in experiments A and B and, therefore, a slight decrease in atmospheric pCO_2 (~1.5 μatm) results, relative to the glacial level (Fig. 3a). In the CSATL biological carbon fixation during the MWE exceeds the glacial level (Fig. 5a) in experiments A, B, and D because some of the excess PO_4 in the deep water of the CSATL (Fig. 4) diffuses into the surface of the CSATL and leads to an increase in productivity during the MWE; however, compared with experiments A and B a significant change occurs in the temporal evolution of productivity in the CSATL in experiment D. Here, MWE productivity even exceeds the modern level because of the combined effect of larger glacial PO_4 uptake rates and elevated PO_4 concentrations in the surface layer. The transient drop in CSATL productivity during the LGM-to-MWE transition (Fig. 5a) occurs because the shutdown of NADW reduces the advective supply of nutrients. The subsequent rise in productivity between 17.1–16.5 cal. ky B.P. reflects the time scale of the PO_4 transfer into the interior of the CSATL and the diffusive transfer of PO_4 into the surface ocean. The drop in productivity, which occurs in experiment D during the MWE-to-Bølling transition, stems from the accompanying reduction in PO_4 uptake rates.

In summary, all experiments with prognostic formulation of productivity during the MWE (A, B, and D) result in only small variations in atmospheric pCO_2 (± 1 μatm) across the LGM-to-MWE transition. We attribute this model result to the negative "productivity feedback," first identified by Marchal et al. (1998). However, our results indicate only a 17% lowering in productivity in the entire Atlantic Ocean between the Bølling (=MOD) and the MWE in experiment A (cf. Fig. 5a,b), compared with a 40% reduction simulated by Marchal et al. (1998). In addition, our modeling results show that the inference of a meltwater induced productivity drop in the Atlantic Ocean depends largely on the choice of PO_4 uptake rates. Accordingly, productivity in the CSATL during the MWE may have exceeded the modern level [experiment D; this trend, however, is not found in sediment records; Sarnthein et al. (1988)].

To separate the effects of changes in surface-water chemical composition and physical properties on atmospheric pCO_2, we estimated the partial differentials of aqueous pCO_2 (pCO_2(aq)) with respect to DIC, ALK, PO_4, temperature and salinity after each time step of experiment D by finite differences. The globally integrated total differential of pCO_2(aq) tracks changes in model predicted atmospheric pCO_2 (cf. Bacastow 1996) with a root-mean-square error of 1.9 μatm, which is sufficiently small to allow for an

interpretation of the globally integrated partial differentials of pCO_2(aq). Variations in surface-water DIC and ALK, which are linked to changes in circulation, mean tracer concentrations and export production, each affect pCO_2(aq) by more than 80 µatm (relative to LGM; Fig. 3b); however, their combined effect on atmospheric pCO_2 never exceeds ±10 µatm. Salinity-controlled variations of atmospheric pCO_2 amount to –1 µatm during the MWE (freshening of the North Atlantic) and reach a maximum effect of –10 µatm during the Bølling (decrease in mean ocean salinity). While the temperature-driven increase in atmospheric pCO_2 remains below 2 µatm during the MWE, a 41 µatm increase results during the MWE-to-Bølling transition. Accordingly, the net increase in atmospheric pCO_2 during this transition (Fig. 3a, exp. D) can largely be attributed to warming of the ocean surface.

Paleoclimatic proxy data indicate a significant early warming of the Southern Ocean during the MWE (Alley and Clark 1999); hence, the use of glacial SSTs as boundary conditions in the Southern Ocean during the MWE results in an overestimation of CO_2 solubility. Similarly, the use of modern SSTs as surrogate for the Bølling introduces a systematic underestimation of CO_2 solubility in both the North Atlantic, where Bølling SSTs remained slightly below modern levels (cf. Experimental strategy), and the Southern Ocean, where the onset of NADW formation caused a cooling (Blunier et al. 1998; Ninnemann et al. 1999). Furthermore, prior to the first major deglacial meltwater pulse at 14.1 cal. ky B.P. (Fairbanks et al. 1992) our application of modern sea-surface salinity values to the Bølling scenario results in an underestimation of salinity and, hence, an overestimation of CO_2 solubility in surface water. To estimate the net effect of biased temperatures and salinities on atmospheric pCO_2, SST in the SPSOC and PSOC were linearly increased from their glacial value to the average of glacial and modern values between 17.1 and 14.7 cal. ky B.P. (exp. E). Furthermore, the average of glacial and modern SST and salinity were used in each box stack for the Bølling scenario experiment E.

Compared with experiment D, the gradual SST rise in the Southern Ocean induces an increase of atmospheric pCO_2, which amounts to ~10 µatm at the end of the MWE (Fig. 6, exp. E). The combined effect of saltier and cooler sea-surface conditions during the Bølling dampens the pCO_2 increase by ~6 µatm at 13.0 cal. ky B.P. compared with experiment D (cf. Figs. 3a, 6). Between 17.5 and 14.7 cal. ky B.P. modeled atmospheric pCO_2 anomalies depict the general trend which is seen in Antarctic ice-core data (Fig. 6, exp. E). However, the model cannot reproduce the pCO_2 maximum, observed in the ice-core record around 15.6 cal. ky B.P., probably because of the boundary conditions assumed. During the Bølling the model clearly overestimates the anomalies derived from measurements (Fig. 6, exp. E). A likely source

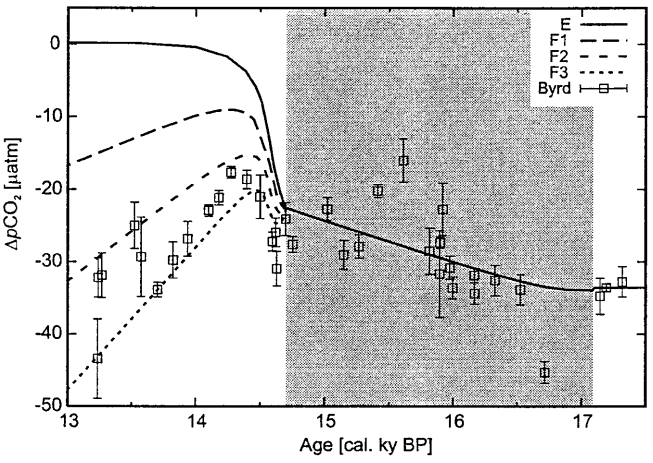

Fig. 6 Deviation of atmospheric pCO_2 from pre-industrial value of 280 µatm in experiments E and F vs pCO_2 anomalies from Byrd ice core (Neftel et al. 1988; Marchal et al. 1999). Ice-core data are detrended between 13–17 cal. ky B.P. (slope=10.7 µatm ky^{-1}; obtained by linear regression between 11–17 cal. ky B.P.) to account for long-term trend in deglacial pCO_2 variation, which is probably linked to variations in the global $CaCO_3$ budget, not included in the model (cf. Archer and Maier-Reimer 1994). A constant was added to the Byrd pCO_2 anomalies to match the modeled LGM deviation. *Shading* shows duration of MWE

for this discrepancy stems from the neglect of carbon sequestration by the terrestrial biosphere during the Bølling (Adams and Faure 1998).

To estimate the potential effect of a terrestrial carbon sink on atmospheric pCO_2 and to test if reconstructed terrestrial carbon sequestration is compatible with the atmospheric pCO_2 evolution, we added a corresponding component to the model that fixes between 0.1–0.3 Gt C $year^{-1}$ between 14.7–13.0 cal. ky B.P. (Adams and Faure 1998). Depending on the sink strength, atmospheric pCO_2 is reduced by 17–48 µatm at 13 cal. ky B.P. in experiments F1–F3 compared with experiment E (Fig. 6). A comparison of the resulting atmospheric pCO_2 anomalies with the ice-core data (Fig. 6) suggests a carbon flux of 0.2–0.3 Gt C $year^{-1}$ into the terrestrial biosphere during the Bølling. Furthermore, this scenario predicts a rise in atmospheric $\delta^{13}C$ by ~0.2‰ between 14.7 and 14.6 cal. ky B.P. [not shown; assuming $\delta^{13}C$ fractionation of –18.7‰ between atmospheric CO_2 and terrestrial carbon (Joos and Bruno 1998)] which is not inconsistent with the atmospheric $\delta^{13}C$ record from Taylor Dome ice core (Smith et al. 1999). [To avoid uncertainties in gas-age ice-age difference (Steig et al. 1998), we used the ice-core record of atmospheric methane from Taylor Dome (Brook et al. 1999) to identify the onset of the Bølling in the $\delta^{13}C$ record (cf. Blunier et al. 1998)]. In experiment F3 a brief drop in atmospheric pCO_2 occurs during the initial phase of the MWE-to-Bølling transition. During this short interval of time, terrestrial carbon demand exceeds the available supply by the ocean (Fig. 6, exp. F3).

As stated previously, the choice of the time span during which the carbon-cycle model is transferred from the MWE to Bølling boundary conditions is somewhat arbitrary. However, even for a transition time of 300 years, the model reaches the interglacial atmospheric pCO_2 level (within ±1 μatm) at 13.7 cal. ky B.P. (based on exp. D, not shown). For a transition time of 20 years atmospheric pCO_2 increases by 18 μatm within 50 years (4 μatm for a 150-year transition time). After this dramatic initial rise, atmospheric pCO_2 reaches the interglacial level (within ±1 μatm) at 13.8 cal. ky B.P. (based on exp. D, not shown). Hence, any improper choice of the transition time is unlikely to invalidate the foregoing results.

Ocean–atmosphere carbon budgets

Changes in oceanic and atmospheric carbon storage during an interglacial-to-glacial cycle, induced by variations in the strength of NADW formation, can be estimated from differences in carbon content of the box model reservoirs. Oceanic carbon budgets were calculated for experiments A–E (experiments F1–F3 are excluded because the carbon inventory in the model decreases due to terrestrial carbon fixation). For the Atlantic Ocean (NATL+CSTAL) carbon budgets were calculated below and above 1.8 km depth ("deep" vs "shallow") in order to facilitate comparison with the benthic $\delta^{13}C$-based estimates of Sarnthein et al. (1994). The robustness of variations in the carbon budgets can be assessed from the consistency in sign and magnitude of carbon storage anomalies between the different experiments.

During the transition from interglacial to glacial mode all experiments indicate excess carbon storage in the deep Atlantic Ocean and Southern Ocean, whereas carbon depletion occurs in the atmosphere (Fig. 7a). However, the model results are ambiguous for both the shallow Atlantic and Indo-Pacific Ocean. In experiments A and B high levels of glacial productivity in the NATL (Fig. 5b) cause excess carbon storage and counterbalance the concomitant carbon depletion in the shallow CSATL. In contrast, reduction of glacial productivity in the NATL in experiments C–E is no longer capable to mask the carbon depletion in the CSATL. Similarly, low glacial productivity in the Indo-Pacific Ocean is responsible for a reduction in carbon storage in experiments A and B, whereas the Indo-Pacific Ocean gains carbon during the transition to the glacial state in experiments C–E because of the higher level of biological carbon fixation. In the deep Atlantic Ocean, the sign of the modeled carbon storage anomaly agrees with the estimate of Sarnthein et al. (1994; Fig. 7a), in contrast to the magnitudes which differ by 28% (exp. C) to 43% (exp. E). Possibly, these discrepancies arises from simply extrapolating reconstructed data from the eastern Atlantic (Sarnthein et al. 1994) to the entire Atlantic. Carbon depletion in the shallow Atlantic in the most realistic experiments D (–8 Gt C) and E (–11 Gt C) agree in both sign and magnitude with the data-derived estimate of Sarnthein et al. (1994). Despite its lower rate of formation, the glacial production of NADW is able to sustain pronounced differences in deep-water DIC concentration and $\delta^{13}C$ between the Atlantic Ocean and the Indo-Pacific Ocean (Fig. 8).

In contrast, the cessation of NADW formation during LGM-to-MWE transition implies that the deep-water DIC concentration difference between the Atlantic and Indo-Pacific oceans almost vanishes in all simulations (Fig. 8a). Similarly, the corresponding deep-water $\delta^{13}C$ difference (Fig. 8b) varies only slightly around 0‰. This major change in global deep-water chemistry is accompanied by a prominent increase in carbon storage in the entire Atlantic [77 Gt C (exp. A) to 93 Gt C (exp. D)] and a carbon loss in the Indo-Pacific and Southern oceans (Fig. 7b). However, as outlined previously, this massive reorganization of the size of the oceanic carbon reservoirs remains largely internal to the global ocean and has only a marginal effect on the carbon content of the atmosphere. Apart from the change in atmospheric carbon storage, signs of modeled anomalies do not

Fig. 7a–c Variations (minimum/maximum values) in carbon storage (Gt C) over an interglacial–glacial cycle in experiments A–E. Reservoirs: atmosphere (*ATM*), Atlantic Ocean (*ATL*=CSATL+NATL), Southern Ocean (*SOC*=SPSOC+PSOC) and Indo-Pacific Oean (*INDPAC*). Paleoceanographic estimates (numbers in parentheses) are deduced from benthic $\delta^{13}C$ values from the eastern Atlantic (60°N–30°S; Sarnthein et al. 1994) and have been extrapolated to the entire Atlantic Ocean. *Dark shading* indicates carbon depletion, whereas *light shading* indicates inconsistent sign of carbon storage anomalies in the experiments

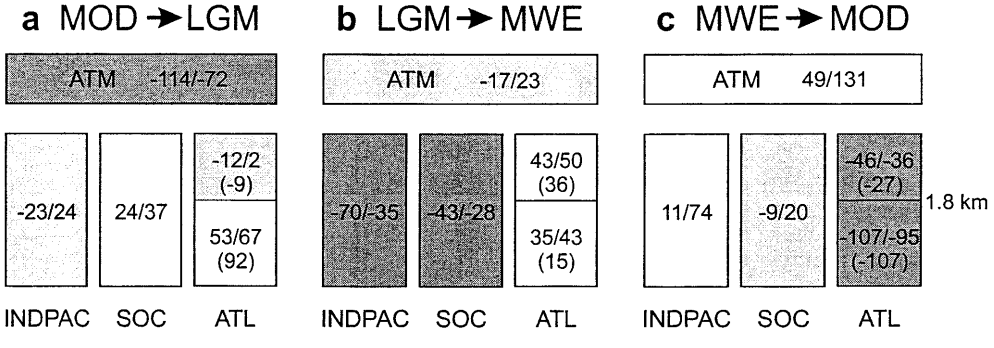

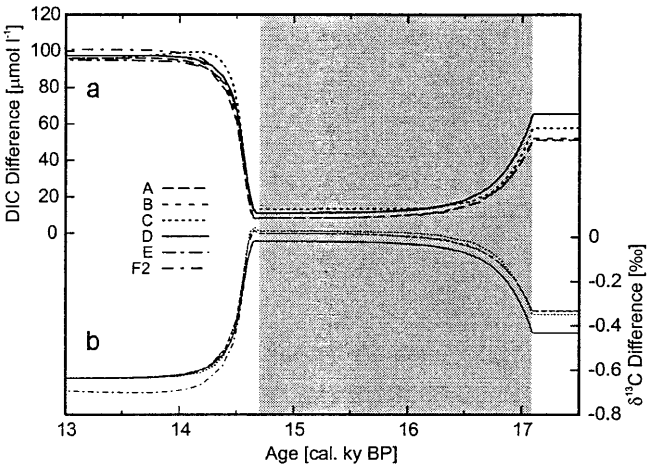

Fig. 8a,b Inter-oceanic concentration differences. **a** Deglacial evolution of DIC concentration difference between INDPAC and CSATL (2 km depth) in experiments A–F; **b** same as **a** but for $\delta^{13}C$. *Shading* shows duration of MWE

vary between the various experiments and are therefore considered as robust (Fig. 7b).

In the shallow MWE Atlantic the predicted amount of excess carbon compares well with the estimate of Sarnthein et al. (1994), whereas the model overestimates the data-derived anomaly in the deep Atlantic Ocean by more than a factor of two (Fig. 7b). The carbon depletion in the Indo-Pacific Ocean is restricted to depths above 1.8 km and goes along with an increase in carbonate ion concentration by 6 µmol l^{-1} (average from experiments A–E in 1.5 km depth, not shown) and, hence, agrees with enhanced carbonate preservation in intermediate water of the Pacific Ocean during the deglacial meltwater event (Berger 1977; Chen et al. 1997).

During the subsequent transition from meltwater to interglacial circulation mode, the model predicts a carbon loss between 131 Gt C (exp. E) and 153 Gt C (exp. C) from the entire Atlantic Ocean. Beside the atmosphere, the Indo-Pacific Ocean gains most of the carbon released from the Atlantic Ocean (Fig. 7c). Depending on the parameterization of productivity, the Southern Ocean acts either as sink (experiments A and B) or source (experiments C–E) for carbon during the transition to the interglacial mode. Since modeled and estimated (Sarnthein et al. 1994) carbon storage anomalies in the deep Atlantic Ocean are in good agreement (Fig. 7c), it appears that the overestimation of excess carbon in the deep Atlantic Ocean during the LGM-to-MWE transition (Fig. 7b) originates from underestimating the carbon storage in glacial Atlantic deep water by the model.

In summary, two independent methods – modeling and paleoceanographic reconstructions (Sarnthein et al. 1994) – result in comparable carbon-storage anomalies in the Atlantic Ocean during an interglacial–glacial cycle (Fig. 7). Considering the difficulties to estimate the amount of anthropogenic carbon in the Atlantic Ocean (Gruber 1998) this agreement may be fortuitous; however, the interglacial-to-glacial variations in Atlantic carbon storage probably exceed the modern uptake of anthropogenic carbon (Gruber 1998) by a factor of 2–3 and hence can be more easily detected and quantified.

Conclusions

Similar to inferences drawn from benthic $\delta^{13}C$ data (Sarnthein et al. 1994) our OGCM results support at least three modes of Atlantic thermohaline circulation, which formed over the transition from the LGM to the Holocene: (a) a glacial mode, which depicts an active, although weaker NADW formation than at present; (b) a meltwater mode, characterized by the complete absence of NADW; and (c) the present interglacial mode.

The intention of the sensitivity experiments with the carbon-cycle model is to quantify changes in Ocean–atmosphere carbon budgets, linked to the three different oceanic circulation modes, during the early part of the last deglaciation. Since the OGCM is forced by modern and reconstructed boundary conditions for three selected time intervals, our model setup cannot capture the transient response of the ocean during the Heinrich event 1 meltwater perturbation. Likewise, by imposing transition times between the three circulation modes in the experiments with the carbon-cycle model, characteristic response times of the carbon cycle upon the meltwater perturbation cannot be resolved. Our results should therefore be considered supplementary to transient-type sensitivity experiments in which the present-day state of the ocean is perturbed by freshwater pulses, the magnitude and spatial-temporal evolution of which are not well constrained by available data. Moreover, since a considerable fraction of changes in atmospheric pCO_2 is controlled by variations in SST (cf. Fig. 3b), the modeled rise in atmospheric pCO_2 at the Heinrich event 1 to Bølling transition should not be extrapolated to the rise in pCO_2 linked to the cessation of previous Heinrich events, since associated SSTs (Cayre et al. 1999; Chapman and Maslin 1999) were considerably lower than during the last deglaciation.

When forced by the OGCM results, our carbon cycle box model explains 34–40 µatm of the observed 80 µatm interglacial-to-glacial shift in atmospheric pCO_2 (except for exp. C: –53 µatm). While the direct effect of glacial ocean circulation accounts for 18% of the total variation in modeled atmospheric pCO_2, the remaining contributions stem from indirect effects, i.e., CO_2 solubility because of changes in SST and salinity (72%) and the ratio between biological carbon fixation and upwelling of DIC-rich water (10%; experiment D). This finding is in harmony with 3D mod-

eling results (Heinze and Hasselmann 1993; Heinze 1994) which showed the important role of indirect effects on atmospheric pCO_2.

Compared to the LGM mode, the cessation of NADW formation during the MWE has only a minor effect on atmospheric pCO_2 (~±1µatm) since a concomitant drop in global export production stabilizes the atmospheric carbon content (experiments A, B, and D). Although our experiments support the existence of a negative "productivity feedback," as identified by Marchal et al. (1998), the meltwater induced reduction in global productivity is by a factor of two smaller than in the corresponding simulation of Marchal et al. (1998). In contrast to the small change in atmospheric carbon content, our model predicts a massive reorganization of oceanic carbon pools during the transition from the LGM to the MWE mode; in particular, 85±8 Gt C are transferred from the Indo-Pacific and Southern Oceans to the Atlantic Ocean. This carbon transfer almost levels the deep-water DIC concentration difference between the Atlantic and Indo-Pacific Oceans.

During the transition from meltwater to interglacial circulation mode, approximately 142±11 Gt C are released from the Atlantic Ocean. The onset of NADW formation after a meltwater event has the potential to raise atmospheric pCO_2 by 38±3 µatm on a centennial time scale (experiments A, B, and D), equivalent to ~50% of the man-made pCO_2 increase. Across the MWE-to-Bølling transition the possible atmospheric pCO_2 increase was, however, mitigated by the gradual warming of the Southern Ocean during the MWE and by terrestrial carbon sequestration (0.2–0.3 Gt C $year^{-1}$) during the Bølling. This scenario is consistent with pCO_2 measurements from the Byrd ice core.

Acknowledgements We greatly appreciate the reviewers' comments which helped to improve the paper. M. Schulz acknowledges various suggestions by W.H. Berger during a 6-month visit to SIO. This work was funded by the DFG within the framework of the SFB 313 and received further support by the "Nationales Klimaforschungsprogramm" of the BMBF.

References

Adams JM, Faure H (1998) A new estimate of changing carbon storage on land since the last glacial maximum, based on global land ecosystem reconstruction. Global Planet Change 17:3–24

Alley RB, Clark PU (1999) The deglaciation of the northern hemisphere: a global perspective. Annu Rev Earth Planet Sci 27:149–182

Alley RB, Meese DA, Shuman CA, Gow AJ, Taylor KC, Grootes PM, White JWC, Ram M, Waddington ED, Mayewski PA, Zielinski GA (1993) Abrupt increase in Greenland snow accumulation at the end of the Younger Dryas event. Nature 362:527–529

Anderson LA, Sarmiento JL (1994) Redfield ratios of remineralization determined by nutrient data analysis. Glob Biogeochem Cycles 8:65–80

Archer D, Maier-Reimer E (1994) Effect of deep-sea sedimentary calcite preservation on atmospheric CO_2 concentration. Nature 367:260–263

Atkinson TC, Briffa KR, Coope GR (1987) Seasonal temperatures in Britain during the past 22,000 years, reconstructed using beetle remains. Nature 325:587–592

Bacastow R (1996) The effect of temperature change of the warm surface waters of the oceans on atmospheric CO_2. Glob Biogeochem Cycles 10:319–333

Bainbridge AE (ed) (1981) GEOSECS Atlantic Expedition, vol 1. Hydrographic data 1972–1973. U.S. Government Printing Office, Washington, D.C., pp 1–121

Bainbridge AE (1982a) GEOSECS Indian Ocean Expedition, vol 5. Hydrographic data 1977–1978. U.S. Government Printing Office, Washington, D.C., pp 1–48

Bainbridge AE (1982b) GEOSECS Pacific Expedition, vol 3. Hydrographic data 1973–1974. U.S. Government Printing Office, Washington, D.C., pp 1–137

Barnola JM, Raynaud D, Korotkevich YS, Lorius C (1987) Vostok ice core provides 160,000-year record of atmospheric CO_2. Nature 329:408–414

Berger WH (1977) Deep-sea carbonate and the deglaciation preservation spike in pteropods and foraminifera. Nature 269:301–304

Blunier T, Chappellaz J, Schwander J, Dällenbach A, Stauffer B, Stocker TF, Raynaud D, Jouzel J, Clausen HB, Hammer CU, Johnsen SJ (1998) Asynchrony of Antarctic and Greenland climate change during the last glacial period. Nature 394:739–743

Bolin B (ed) (1981) SCOPE, 16: Carbon cycle modelling. Wiley, Chichester, pp 1–389

Bond G, Heinrich H, Broecker W, Labeyrie L, McManus J, Andrews J, Huon S, Jantschik R, Clasen S, Simet C, Tedesco K, Klas M, Bonani G, Ivy S (1992) Evidence for massive discharges of icebergs into the North Atlantic ocean during the last glacial period. Nature 360:245–249

Boyle EA (1992) Cadmium and $\delta^{13}C$ paleochemical ocean distributions during the stage 2 glacial maximum. Annu Rev Earth Planet Sci 20:245–287

Boyle EA, Keigwin LD (1987) North Atlantic thermohaline circulation during the past 20,000 years linked to high-latitude surface temperature. Nature 330:35–40

Brook EJ, Harder S, Severinghaus J, Bender M (1999) Atmospheric methane and millennial-scale climate change. Am Geophys Union Geophys Monogr 112:165–175

Bryan K (1969) A numerical method for the study of the circulation of the world ocean. J Comput Phys 4:347–376

Bryan F (1986) High-latitude salinity effects and interhemispheric thermohaline circulation. Nature 323:301–304

Campin J-M, Fichefet T, Duplessy J-C (1999) Problems with using radiocarbon to infer ocean ventilation rates for past and present climates. Earth Planet Sci Lett 165:17–24

Cayre O, Lancelot Y, Vincent E (1999) Paleoceanographic reconstructions from planktonic foraminifera off the Iberian Margin: temperature, salinity, and Heinrich events. Paleoceanography 14:384–396

Chapman MR, Maslin MA (1999) Low-latitude forcing of meridional temperature and salinity gradients in the subpolar North Atlantic and the growth of glacial ice sheets. Geology 27:875–878

Charles CD, Fairbanks RG (1992) Evidence from Southern Ocean sediments for the effect of North Atlantic deep-water flux on climate. Nature 355:416–419

Chen MT, Huang CY, Wei KY (1997) 25,000-year late Quaternary records of carbonate preservation in the South China Sea. Palaeogeogr Palaeoclimatol Palaeoecol 129:155–169

Cox MD (1984) A primitive equation, 3-dimensional model of the ocean. Geophysical Fluid Dynamics Laboratory, Princeton University, Princeton, GFDL Ocean Group Tech Rep 1:1–103

Dansgaard W, Johnsen SJ, Clausen HB, Dahl-Jensen D, Gundestrup NS, Hammer CU, Hvidberg CS, Steffensen JP, Sveinbjörnsdottir AE, Jouzel J, Bond G (1993) Evidence for general instability of past climate from a 250-kyr ice-core record. Nature 364:218–220

Dugdale RC (1967) Nutrient limitation in the sea: dynamics, identification, and significance. Limnol Oceanogr 12:685–695

Duplessy J-C (1982) Glacial to interglacial contrasts in the northern Indian Ocean. Nature 295:494–498

Duplessy JC, Shackleton NJ, Fairbanks RG, Labeyrie L, Oppo D, Kallel N (1988) Deepwater source variations during the last climatic cycle and their impact on the global deepwater circulation. Paleoceanography 3:343–360

Duplessy J-C, Arnold M, Bard E, Julliet-Lerclerc A, Kallel N, Labeyrie L (1989) AMS ^{14}C study of transient events and of the ventilation rate of the Pacific intermediate water during the last deglaciation. Radiocarbon 31:493–502

Duplessy JC, Labeyrie L, Arnold M, Paterne M, Duprat J, van Weering TCE (1992) Changes in surface salinity of the North Atlantic Ocean during the last deglaciation. Nature 358:485–488

Duplessy JC, Labeyrie L, Paterne M, Hovine S, Fichefet T, Duprat J, Labracherie M (1996) High latitude deep water sources during the last glacial maximum and the intensity of the global oceanic circulation. In: Wefer G, Berger WH, Siedler G, Webb DJ (eds) The South Atlantic. Springer, Berlin Heidelberg New York, pp 445–460

Fairbanks RG, Charles CD, Wright JD (1992) Origin of global meltwater pulses. In: Taylor RE, Long A, Kra RS (eds) Radiocarbon after four decades. Springer, Berlin Heidelberg New York, pp 473–500

François R, Altabet MA, Yu E-F, Sigman DM, Bacon MP, Frank M, Bohrmann G, Bareille G, Labeyrie LD (1997) Contribution of Southern Ocean surface-water stratification to low atmospheric CO_2 concentrations during the last glacial period. Nature 389:929–935

Ganopolski A, Rahmstorf S, Petoukhov V, Claussen M (1998) Simulation of modern and glacial climates with a coupled global model of intermediate complexity. Nature 391:351–356

Gruber N (1998) Anthropogenic CO_2 in the Atlantic Ocean. Global Biogeochem Cycles 12:165–191

Guiot J, Beaulieu JL de, Cheddadi R, David F, Ponel P, Reille M (1993) The climate in western Europe during the last glacial/interglacial cycle derived from pollen and insect remains. Palaeogeogr Palaeoclimatol Palaeoecol 103:73–93

Heinze C (1990) Zur Erniedrigung des atmosphärischen Kohlendioxidgehalts durch den Weltozean während der letzten Eiszeit. Max-Planck-Institut für Meteorologie, Hamburg, Examensarbeit 3:1–180

Heinze C (1994) Glacial ocean carbon cycle modeling. In: Zahn R, Pedersen TF, Kaminski MA, Labeyrie LD (eds) Carbon cycling in the glacial ocean: constraints on the ocean's role in global change. Springer, Berlin Heidelberg New York, pp 15–37

Heinze C, Hasselmann K (1993) Inverse multiparameter modeling of paleoclimate carbon cycle indices. Quaternary Res 40:281–296

Herguera JC, Berger WH (1994) Glacial to postglacial drop in productivity in the western equatorial Pacific: mixing rate vs nutrient concentrations. Geology 22:629–632

Jansen E, Veum T (1990) Evidence for two-step deglaciation and its impact on North Atlantic deep-water circulation. Nature 343:612–616

Jasper JP, Hayes JM, Mix AC, Prahl FG (1994) Photosynthetic fractionation of ^{13}C and concentrations of dissolved CO_2 in the central equatorial Pacific during the last 255,000 years. Paleoceanography 9:781–798

Jones GA, Keigwin LD (1988) Evidence from Fram Strait (78°N) for early deglaciation. Nature 336:56–59

Joos F, Bruno M (1998) Long-term variability of the terrestrial and oceanic carbon sinks and the budgets of the carbon isotopes ^{13}C and ^{14}C. Global Biogeochem Cycles 12:277–295

Keeling CD, Bolin B (1967) The simultaneous use of chemical tracers in oceanic studies. I. General theory of reservoir models. Tellus 19:566–581

Keigwin LD, Jones GA, Lehman SJ (1991) Deglacial meltwater discharge, North Atlantic deep circulation and abrupt climate change. J Geophys Res C96:16811–16826

Keir RS (1988) On the late Pleistocene ocean chemistry and circulation. Paleoceanography 3:413–445

Kennett JP, Ingram BL (1995) A 20,000-year record of ocean circulation and climate change from the Santa Barbara basin. Nature 377:510–514

Koç Karpuz N, Jansen E (1992) A high resolution diatom record of the last deglaciation from the SE Norwegian Sea: documentation of rapid climatic changes. Paleoceanography 7:499–520

Kumar N, Anderson RF, Mortlock RA, Froelich PN, Kubik P, Dittrich-Hannen B, Suter M (1995) Increased biological productivity and export production in the glacial Southern Ocean. Nature 378:675–680

Lalli CM, Parsons T (1993) Biological oceanography. Pergamon Press, Oxford, pp 1–301

Lehman SJ, Keigwin LD (1992) Sudden changes in North Atlantic circulation during the last deglaciation. Nature 356:757–762

Lehman SJ, Jones GA, Keigwin LD, Andersen ES, Butenko G, Östmo S-R (1991) Initiation of Fennoscandina ice-sheet retreat during the last glaciation. Nature 349:513–516

Levitus S, Boyer TP (1994) World Ocean Atlas 1994, vol 4. Temperature. NOAA National Environmental Satellite Data and Information Service, Washington, D.C., pp 1–117

Levitus S, Burgett R, Boyer TP (1994) World Ocean Atlas 1994, vol 3. Salinity. NOAA National Environmental Satellite Data and Information Service, Washington, D.C., pp 1–99

Lorenz S, Grieger B, Helbig P, Herterich K (1996) Investigating the sensitivity of the atmospheric general circulation model ECHAM 3 to paleoclimatic boundary conditions. Geol Rundsch 85:513–524

Lyle M (1988) Climatically forced organic carbon burial in equatorial Atlantic and Pacific oceans. Nature 335:529–532

Macdonald AM (1993) Property fluxes at 30°S and their implications for the Pacific–Indian throughflow and the global heat budget. J Geophys Res C98:6851–6868

Macdonald AM, Wunsch C (1996) An estimate of global ocean circulation and heat fluxes. Nature 382:436–439

Manabe S, Stouffer RJ (1995) Simulation of abrupt climate change induced by freshwater input to the North Atlantic Ocean. Nature 378:165–167

Manighetti B, McCave IN (1995) Depositional fluxes, palaeoproductivity, and ice rafting in the NE Atlantic over the past 30 ka. Paleoceanography 10:579–592

Marchal O, Stocker TF, Joos F (1998) Impact of oceanic reorganizations on the ocean carbon cycle and atmospheric carbon dioxide content. Paleoceanography 13:225–244

Marchal O, Stocker TF, Joos F, Indermühle A, Blunier T, Tschumi J (1999) Modelling the concentration of atmospheric CO_2 during the Younger Dryas climate event. Clim Dyn 15:341–354

Marchitto TM, Curry WB, Oppo DW (1998) Millennial-scale changes in North Atlantic circulation since the last glaciation. Nature 393:557–561

Michel E (1991) L'ocean au dernier maximum glaciaire: Le cycle du carbone et la circulation. Constraintes isotopiques et modelisation. Doctoral Thesis, Universite de Paris-Sud, Centre d'Orsay, pp 1–191

Mix AC (1989) Influence of productivity variations on long-term atmospheric CO_2. Nature 337:541–544

Murray RW, Leinen M, Isern AR (1993) Biogenic flux of Al to sediment in the central equatorial Pacific Ocean: evidence for increased productivity during glacial periods. Paleoceanography 8:651–670

Najjar RG, Sarmiento JL, Toggweiler JR (1992) Downward transport and fate of organic matter in the ocean: simulations with a general circulation model. Global Biogeochem Cycles 6:45–76

Neftel A, Oeschger H, Staffelbach T, Stauffer B (1988) CO_2 record in Byrd ice core 50,000–5,000 years B.P. Nature 331:609–611

Ninnemann US, Charles CD, Hodell DA (1999) Origin of global millennial scale climate events: constraints from the Southern Ocean deep sea sedimentary record. Am Geophys Union Geophys Monogr 112:99–112

Nürnberg CC, Bohrmann G, Schlüter M, Frank M (1997) Barium accumulation in the Atlantic sector of the Southern Ocean: results from 190,000-year records. Paleoceanography 12:594–603

Oppo DW, Fairbanks RG (1987) Variability in the deep and intermediate water circulation of the Atlantic Ocean during the past 25,000 years: Northern hemisphere modulation of the Southern Ocean. Earth Planet Sci Lett 86:1–15

Pacanowski R, Dixon K, Rosati A (1993) The GFDL modular ocean model user's guide. Geophysical Fluid Dynamics Laboratory, Princeton University, Princeton, GFDL Ocean Group Tech Rep 2

Paillard D, Ghil M, Letreut H (1993) Dissolved organic matter and the glacial–interglacial pCO_2 problem. Global Biogeochem Cycles 7:901–914

Pedersen TF, Nielsen B, Pickering M (1991) Timing of late Quaternary productivity pulses in the Panama basin and implications for atmospheric CO_2. Paleoceanography 6:657–677

Peng T-H, Takahashi T, Broecker WS, Olaffson J (1987) Seasonal variability of carbon dioxide, nutrients and oxygen in the northern North Atlantic surface water: observations and a model. Tellus 39B:439–458

Rahmstorf S, Marotzke J, Willebrand J (1996) Stability of the thermohaline circulation. In: Krauss W (ed) The warmwatersphere of the North Atlantic Ocean. Borntraeger, Berlin, pp 129–157

Reid JR (1996) On the circulation of the South Atlantic Ocean. In: Wefer G, Berger WH, Siedler G, Webb DJ (eds) The South Atlantic. Springer, Berlin Heidelberg New York, pp 13–44

Sancetta C (1992) Primary production in the glacial North Atlantic and North Pacific oceans. Nature 360:249–251

Sarnthein M, Winn K, Duplessy J-C, Fontugne MR (1988) Global variations of surface ocean productivity in low and mid latitudes: influence on CO_2 reservoirs of the deep ocean and atmosphere during the last 21,000 years. Paleoceanography 3:361–399

Sarnthein M, Jansen E, Arnold M, Duplessy JC, Erlenkeuser H, Flatoy A, Veum T, Vogelsang E, Weinelt MS (1992) $\delta^{18}O$ time-slice reconstruction of meltwater anomalies at Termination I in the North Atlantic between 50 and 80°N. NATO ASI Series 12:183–200

Sarnthein M, Winn K, Jung SJA, Duplessy JC, Labeyrie L, Erlenkeuser H, Ganssen G (1994) Changes in East Atlantic deepwater circulation over the last 30,000 years – 8 time slice reconstructions. Paleoceanography 9:209–267

Sarnthein M, Jansen E, Weinelt M, Arnold M, Duplessy JC, Erlenkeuser H, Flatoy A, Johannessen G, Johannessen T, Jung S, Koc N, Labeyrie L, Maslin M, Pflaumann U, Schulz H (1995) Variations in Atlantic surface ocean paleoceanography, 50°–80°N: a time-slice record of the last 30,000 years. Paleoceanography 10:1063–1094

Sarnthein M, Stattegger K, Dreger D, Erlenkeuser H, Grootes P, Haupt B, Jung S, Kiefer T, Kuhnt W, Pflaumann U, Schäfer-Neth C, Schulz H, Schulz M, Seidov D, Simstich J, van Kreveld S, Vogelsang E, Völker A, Weinelt M (in press) Fundamental modes and abrupt changes in North Atlantic circulation and climate over the last 60 ky: concepts, reconstructions and numerical modeling. In: Schäfer P, Ritzrau W, Schlüter M, Thiede J (eds) The Northern North Atlantic: a changing environment. Springer, Berlin Heidelberg New York

Schmitz WJ (1995) On the interbasin-scale thermohaline circulation. Rev Geophys 33:151–173

Schulz H (1995) Meeresoberflächentemperaturen vor 10.000 Jahren – Auswirkungen des frühholozänen Insolationsmaximums. Ber Rep Geol-Paläontol Inst Univ Kiel 73:1–156

Schulz M (1998) Numerische Modellexperimente zur Veränderung des Ozean-Atmospäre-Kohlenstoffkreislaufes während der letzten 21000 Jahre: Der Einfluss von Variationen der thermohalinen Ozeanzirkulation. Ber SFB 313, Univ Kiel 74:1–177

Seidov D, Haupt BJ (1997) Global ocean thermohaline conveyor at present and in the late Quaternary. Geophys Res Lett 24:2817–2820

Seidov D, Haupt BJ (1999) Numerical study of glacial and meltwater global ocean thermohaline conveyor. In: Harff J, Lemke W, Stattegger K (eds) Computerized modeling of sedimentary systems. Springer, Berlin Heidelberg New York, pp 79–113

Seidov D, Sarnthein M, Stattegger K, Prien R, Weinelt M (1996) North Atlantic ocean circulation during the last glacial maximum and subsequent meltwater event: a numerical model. J Geophys Res C101:16305–16332

Siegenthaler U, Wenk T (1984) Rapid atmospheric CO_2 variations and ocean circulation. Nature 308:624–626

Smith HJ, Fischer H, Wahlen M, Mastroianni D, Deck B (1999) Dual modes of the carbon cycle since the Last Glacial Maximum. Nature 400:248–250

Steig EJ, Brook EJ, White JWC, Sucher CM, Bender ML, Lehman SJ, Morse DL, Waddington ED, Clow GD (1998) Synchronous climate changes in Antarctica and the North Atlantic. Science 282:92–95

Stocker TF, Broecker WS, Wright DG (1994) Carbon uptake experiments with a zonally averaged global ocean circulation model. Tellus 46B:103–122

Veum T, Jansen E, Arnold M, Beyer I, Duplessy J-C (1992) Water mass exchange between the North Atlantic and the Norwegian Sea during the past 28,000 years. Nature 356:783–785

Weaver AJ, Eby M, Augustus FF, Wiebe EC (1998) Simulated influence of carbon dioxide, orbital forcing and ice sheets on the climate of the Last Glacial Maximum. Nature 394:847–853

Winguth AME, Archer D, Duplessy JC, Maier-Reimer E, Mikolajewicz U (1999) Sensitivity of paleonutrient tracer distributions and deep-sea circulation to glacial boundary conditions. Paleoceanography 14:304–323

Yu EF, Francois R, Bacon MP (1996) Similar rates of modern and last-glacial ocean thermohaline circulation inferred from radiochemical data. Nature 379:689–694

Zhang J, Quay PD, Wilbur DO (1995) Carbon isotope fractionation during gas-water exchange and dissolution of CO_2. Geochim Cosmochim Acta 59:107–114